

Metrology for block copolymer directed self-assembly structures using Mueller matrix-based scatterometry

Dhairya J. Dixit
Vimal Kamineni
Richard Farrell
Erik R. Hosler
Moshe Preil
Joseph Race
Brennan Peterson
Alain C. Diebold

Metrology for block copolymer directed self-assembly structures using Mueller matrix-based scatterometry

Dhairya J. Dixit,^{a,*} Vimal Kamineni,^b Richard Farrell,^b Erik R. Hosler,^b Moshe Preil,^c Joseph Race,^d Brennan Peterson,^d and Alain C. Diebold^a

^aCollege of Nanoscale Science & Engineering, 257 Fuller Road, Albany, New York 12203, United States

^bGLOBALFOUNDRIES U.S. Inc., 255 Fuller Road, Suite 280, Albany, New York 12203, United States

^cGLOBALFOUNDRIES U.S. Inc., 1050 Arques Avenue, Sunnyvale, California 94085, United States

^dNanometrics, 1550 Buckeye Drive, Milpitas, California 95035, United States

Abstract. Patterning based on directed self-assembly (DSA) of block copolymer (BCP) has been demonstrated to be a cost-effective manufacturing technique for advanced sub-20-nm structures. This paper describes the application of Mueller matrix spectroscopic ellipsometry (MMSE) based scatterometry to optically characterize polystyrene-*b*-polymethylmethacrylate patterns and Si fins fabricated with DSA. A regression-based (inverse-problem) approach is used to calculate the line-width, line-shape, sidewall-angle, and thickness of the DSA structures. In addition, anisotropy and depolarization calculations are used to determine the sensitivity of MMSE to DSA pattern defectivity. As pattern order decreases, the mean squared error value increases, depolarization value increases, and anisotropy value decreases. These specific trends are used in the current work as a method to judge the degree of alignment of the DSA patterns across the wafer. © The Authors. Published by SPIE under a Creative Commons Attribution 3.0 Unported License. Distribution or reproduction of this work in whole or in part requires full attribution of the original publication, including its DOI. [DOI: [10.1117/1.JMM.14.2.021102](https://doi.org/10.1117/1.JMM.14.2.021102)]

Keywords: directed self-assembly; scatterometry; optical critical dimension; Mueller matrix; ellipsometry; block copolymer.

Paper 14120SSP received Aug. 1, 2014; accepted for publication Dec. 16, 2014; published online Apr. 10, 2015.

1 Introduction

Although block copolymer (BCP) directed self-assembly (DSA) based patterning has demonstrated the capability of processing with high resolution, throughput, and cost effectiveness, advances in critical dimension (CD) and overlay measurement as well as rapid defect characterization are required.¹ Both scatterometry and critical dimension scanning electron microscopy (CD-SEM) are routinely used for inline dimensional metrology. CD-SEM inspection is limited, as it does not easily provide detailed line-shape information, whereas Mueller matrix spectroscopic ellipsometry (MMSE) based scatterometry has the capability of measuring important feature dimensions, including: line-width, line-shape, sidewall-angle, and thickness of the patterned samples quickly and nondestructively.²

This paper describes the application of MMSE-based scatterometry to characterize structures at various integration steps of the BCP DSA based patterning process. Section 1.1 contains a brief introduction of the resist trim and neutral brush (RTNB) and neutral layer lift off (NLLO) DSA chemoeptaxy processes used to fabricate line-space patterns, which may be used to fabricate Si fins. In Sec. 1.2, the basic experimental background is given, along with a description of the multiazimuth MMSE based scatterometry method, depolarization, and anisotropy coefficient calculation methods. Detailed MMSE data analysis, scatterometry results, and defectivity analysis of unetched samples [referred to as polystyrene-*b*-polymethylmethacrylate (PS-*b*-PMMA) patterns], etched samples (referred to as PS line-space patterns), and Si fin samples are shown in Secs. 2.1, 2.2, and 2.3, respectively.

1.1 Directed Self-Assembly

BCPs can autonomously form regular patterns with well-defined dimensions and periodicity by a minimization of free energy via microphase separation.³ DSA patterning is based on thin film processing with BCPs. Different microphase morphologies (cylinder-forming, lamella forming, etc.) are obtained according to the BCP composition, thereby defining the patterned structures. Two respective process flows, RTNB and NLLO, chemoeptaxy methods are seen in Figs. 1 and 2, respectively. Several key differences are observed in the process flows, for example, the use of cross-linked polystyrene patterns that are attractive toward the PS as RTNB guides and the use of pinning regions formed in the anti-reflective coating layer that are attractive toward the PMMA as the NLLO guides. From the perspective of process simplicity and cost, the NLLO process has some clear advantages over RTNB.¹ Both processes have demonstrated a capability for patterning 300-mm wafers with high-resolution line-space structures.^{1,4–6}

The BCP DSA patterning performance is dependent on underlying prepattern pitch, guide strip CD, variation in chemistry of background materials, and B film thickness. At optimum conditions, parallel defect free DSA PS-*b*-PMMA patterns are obtained. However, as the conditions deviate from optimal, defectivity and disorder are present in the DSA patterns.¹ As the DSA patterns are transferred into the underlying layers for fin formation, similar defects are found in the etched samples. Additional defects may also be present in the Si fin samples due to the etch process.

1.2 Design of Experiment

The polymer samples (PS-*b*-PMMA patterns and PS line-space patterns with a lamellae period of $L_o \sim 28$ nm) measured in this work are fabricated by the RTNB method on a 300-mm wafer. The focus and exposure conditions are

*Address all correspondence to: Dhairya J. Dixit, E-mail: ddixit@sunynconse.com

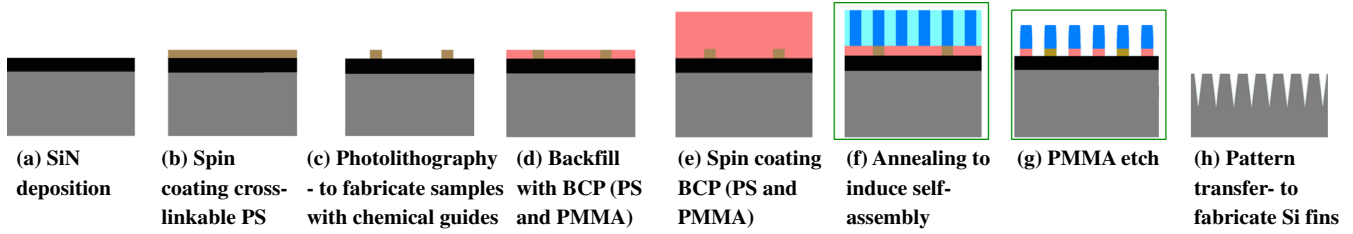


Fig. 1 Outline of the resist trim and neutral brush chemoepitaxy method.

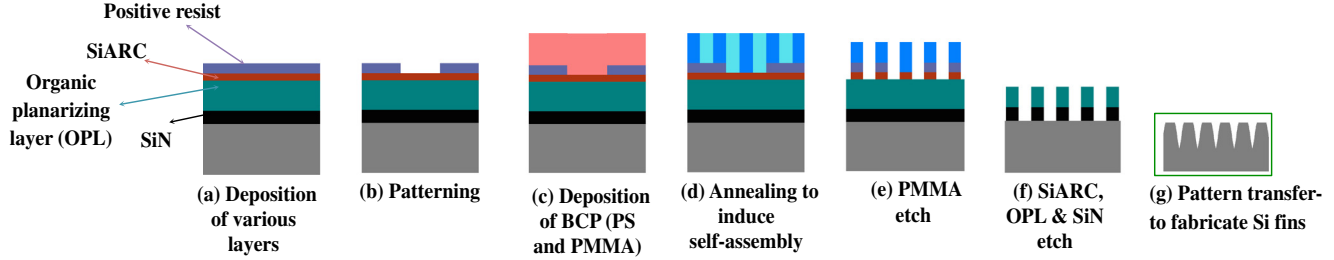


Fig. 2 Outline of the neutral layer lift off chemoepitaxy method (NLLO).

systematically varied across the wafer (referred to as a focus exposure matrix or FEM wafer in this paper) as seen in Fig. 3. For the Si fin samples, the NLLO method is utilized, but the lithography is conducted at the optimal focus and exposure conditions as established by process window analysis.

MMSE data are collected from four different guide pattern pitch macros ($3xL_o$, $4xL_o$, $5xL_o$, $6xL_o$) across the whole wafer at various azimuth angles, δ (0, 45, and 90 deg) over a spectral range between 245 and 1700 nm using a J.A. Woollam RC2® spectroscopic ellipsometer. The spectrometer is capable of collecting all MM elements in parallel with Psi (Ψ) and Delta (Δ) quantities. The angle of incidence (AOI) for all the measurements is fixed at 65 deg for focusing probe measurements, and the azimuth angle is the angle between the grating direction and AOI as shown in Fig. 4. Collecting multiple measurements from the same structure while varying the azimuth angle enhances the amount of spectral information available for modeling.⁷ Traditional spectroscopic ellipsometry (SE) measures the Ψ and Δ parameters by the change in polarization as the incident light scatters from the sample. Ψ and Δ are all that

are required for characterizing a nondepolarizing, optically isotropic, and unpatterned sample.

$$\frac{R_p}{R_s} = \tan \Psi e^{i\Delta}, \quad (1)$$

where

$$\Psi = \tan^{-1} \sqrt{\frac{R_p}{R_s}} \quad \text{and} \quad \Delta = \delta_{R_p} - \delta_{R_s}.$$

Here, R_p , R_s , δ_{R_p} , and δ_{R_s} are the Fresnel reflection coefficients (R) and phase difference of the indicated light polarization, respectively.

The Mueller matrix formalism provides complete information of the interaction (depolarization, scattering effects, anisotropy, etc.) of incident light with the sample.⁷ The Mueller matrix for a depolarizing isotropic sample is seen in Eq. (2)

$$M = \begin{bmatrix} 1 & -N & 0 & 0 \\ -N & 1 & 0 & 0 \\ 0 & 0 & C & S \\ 0 & 0 & -S & C \end{bmatrix}. \quad (2)$$

Here,

$$\begin{aligned} N &= \cos(2\Psi), \\ C &= \sin(2\Psi) \cos(\Delta), \\ S &= \sin(2\Psi) \sin(\Delta). \end{aligned} \quad (3)$$

However, the patterned structures used in integrated circuit manufacturing are often optically anisotropic and structures often depolarize part of the scattered light. Symmetric patterned structures are optically anisotropic. Therefore, measurement at azimuthal angles other than 0 and 90 deg result in nonzero off-diagonal Mueller matrix elements.^{8,9} The resulting nondepolarizing MM is related to the ellipsometric parameters by

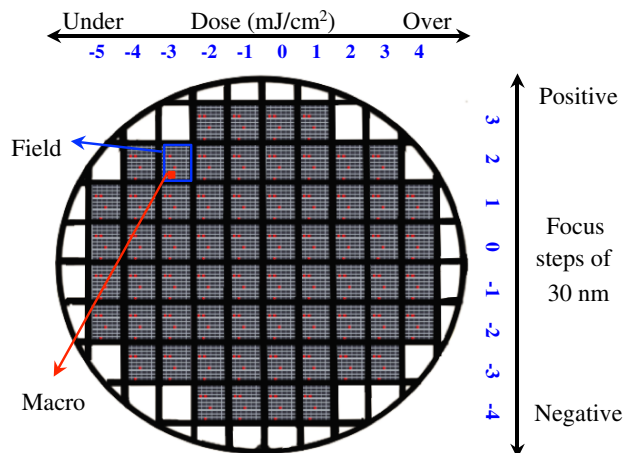


Fig. 3 Across-wafer lithography with focus-exposure variation.

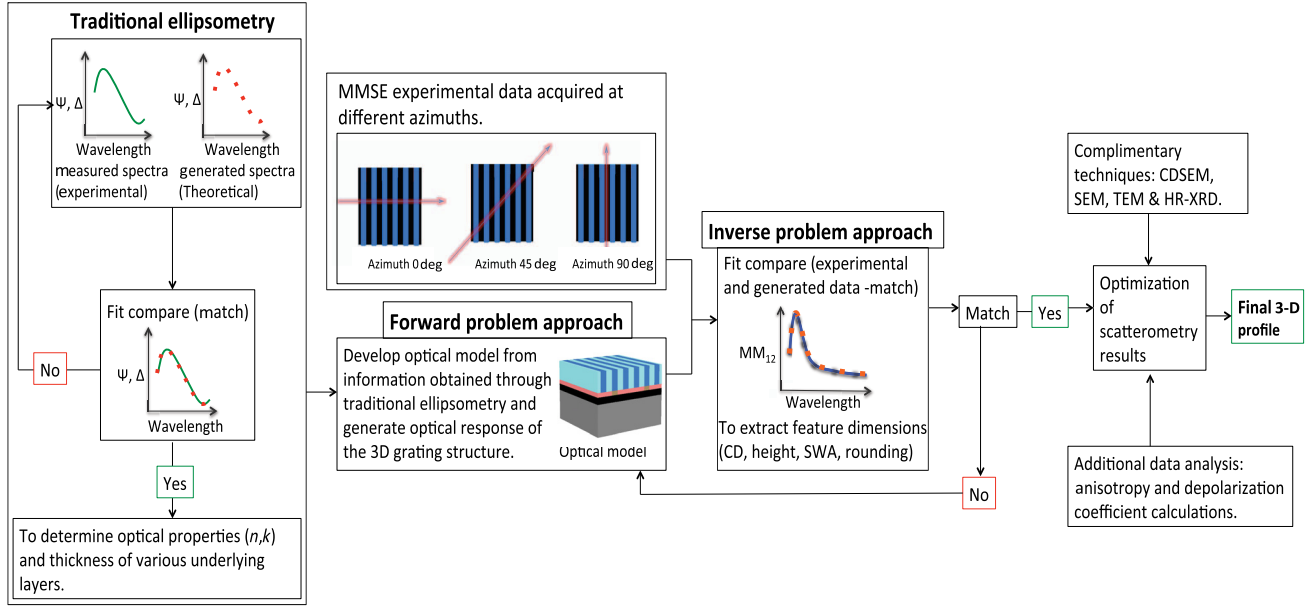


Fig. 4 Overview of the scatterometry method used to evaluate and calculate the feature dimensions.

$$M = \begin{bmatrix} M_{11} & M_{12} & M_{13} & M_{14} \\ M_{21} & M_{22} & M_{23} & M_{24} \\ M_{31} & M_{32} & M_{33} & M_{34} \\ M_{41} & M_{42} & M_{43} & M_{44} \end{bmatrix} \\
 = \begin{bmatrix} 1 & -N - \alpha_{ps} & C_{sp} + \zeta_1 & S_{sp} + \zeta_2 \\ -N - \alpha_{sp} & 1 - \alpha_{sp} - \alpha_{ps} & -C_{sp} + \zeta_1 & -S_{sp} + \zeta_2 \\ C_{ps} + \xi_1 & -C_{ps} + \xi_1 & C_{pp} + \beta_1 & S_{pp} + \beta_2 \\ -S_{ps} + \xi_2 & S_{ps} + \xi_2 & -S_{pp} + \beta_2 & C_{pp} + \beta_1 \end{bmatrix}. \quad (4)$$

Here,

$$\begin{aligned}
 N &= [1 - \tan^2(\psi_{pp}) - \tan^2(\psi_{ps}) - \tan^2(\psi_{sp})]/D \\
 D &= [1 - \tan^2(\psi_{pp}) + \tan^2(\psi_{ps}) + \tan^2(\psi_{sp})] \\
 C &= 2 \tan(\psi_{pp}) \cos(\Delta_{pp})/D \\
 S &= 2 \tan(\psi_{pp}) \sin(\Delta_{pp})/D \\
 S_{ij} &= 2 \tan(\psi_{ij}) \sin(\Delta_{ij})/D \\
 C_{ij} &= 2 \tan(\psi_{ij}) \cos(\Delta_{ij})/D \\
 \alpha_{ij} &= 2 \tan^2(\psi_{ij})/D, \\
 \zeta_1 &= (D/2)(CC_{ps} + SS_{ps}) \\
 \zeta_2 &= (D/2)(CC_{ps} - SS_{ps}) \\
 \xi_1 &= (D/2)(CC_{sp} + SS_{sp}) \\
 \xi_2 &= (D/2)(CC_{sp} - SS_{sp}) \\
 \beta_1 &= (D/2)(C_{ps}C_{sp} + S_{ps}S_{sp}) \\
 \beta_2 &= (D/2)(C_{ps}C_{sp} - S_{ps}S_{sp}). \quad (5)
 \end{aligned}$$

Optical properties (refractive index and extinction coefficient) and the thicknesses of SiN, PS, and PMMA are measured at an earlier process step using SE. These parameters are used in the final structure model to reduce the number of

floating parameters. The optical response of the DSA structure is generated using the forward problem approach and regression based on rigorous coupled wave analysis.¹⁰ The generated optical response is fit to the experimentally measured optical spectra with the help of three-dimensional structural models to extract feature dimensions like CD, height, sidewall-angle, and line-shape using NanoDiffract® software. In order to confirm the results, a repeatability analysis is carried out; MMSE data are collected at nine different spots from each chemical guide pitch macro measured at 0, 45, and 90 deg azimuth angles and the analysis is repeated for each data point.

CD-SEM imaging is conducted as a comparative metric for scatterometry analysis of PS-*b*-PMMA pattern and PS line-space pattern wafers. High-resolution x-ray diffraction measurements, SEM, and transmission electron microscope (TEM) imaging are also conducted as comparative metrics for scatterometry analysis of the Si fins. Additionally, the current work represents a unique application of using mean squared error (MSE), anisotropy, and depolarization values as a method to judge the degree of alignment of the DSA patterns across the wafer. The MSE is used as the criteria to estimate the degree of mismatch between experimental and model-generated MM data and is calculated as follows:

$$\text{MSE} = \frac{1}{(N - M)} \sum_{i=1}^N [y_i - y(x_i)]^2. \quad (6)$$

Here, y_i is the experimental MMSE data, $y(x_i)$ is the generated MMSE data, N is the number of data points, and M is the number of floating parameters.

Depolarization is caused by the incoherent superposition of the optical responses from different sample regions within the probe beam due to presence of nonidealities like surface roughness, inhomogeneity, film-thickness variation, target etch effects, probe beam angular spread, and finite spectral

bandwidth.⁷ Depolarization provides an excellent metric for the degree of defectivity in samples. A depolarization coefficient (D) is calculated from

$$D = M_{11} - \sqrt{\frac{\text{trace}(M \cdot M^T) - (M_{11})^2}{3}}. \quad (7)$$

Here, M and M^T are the Mueller matrix and its transpose, respectively. The value for D ranges from 0 (nondepolarizing) to 1 (perfectly depolarizing).^{11,12}

Calculation of the anisotropy coefficients (α , β , and γ) from experimental MMSE data free of depolarization is very simple and straightforward.¹³ Nondepolarizing MMSE data are retrieved using known mathematical decomposition techniques.¹⁴ Also, it is important to note that full 16 element MMSE data are required to carry out the anisotropy calculations. α , β , and γ are described as the ratios of horizontal linear anisotropy, 45 deg linear anisotropy, and circular anisotropy, respectively. The coefficients are not quantitatively equivalent to the absolute magnitudes of the anisotropies, but rather they are anisotropy ratios relative to the global anisotropy. Anisotropy coefficients are calculated as follows:

$$\begin{aligned} \alpha &= \frac{(M_{12} + M_{21})^2 + (M_{34} - M_{43})^2}{\Sigma} \\ \beta &= \frac{(M_{13} + M_{31})^2 + (M_{24} - M_{42})^2}{\Sigma} \\ \gamma &= \frac{(M_{14} + M_{41})^2 + (M_{23} - M_{32})^2}{\Sigma}. \end{aligned} \quad (8)$$

Here,

$$\begin{aligned} \Sigma &= 3(M_{11})^2 - [(M_{22})^2 + (M_{33})^2 + (M_{44})^2] + 2\Delta \\ \Delta &= (M_{12}M_{21} + M_{13}M_{31} + M_{14}M_{41}) \\ &\quad - (M_{34}M_{43} + M_{24}M_{42} + M_{23}M_{32}). \end{aligned} \quad (9)$$

For a nondepolarizing sample, anisotropy coefficients are related to each other by $\alpha^2 + \beta^2 + \gamma^2 = 1$. The values of the anisotropy coefficients for horizontal linear anisotropy are $\alpha = 1$, $\beta = 0$, and $\gamma = 0$, for 45 deg linear anisotropy, the values are $\alpha = 0$, $\beta = 1$, $\gamma = 0$, and for circular anisotropy, the values are $\alpha = 0$, $\beta = 0$, $\gamma = 1$.

2 Results

2.1 Analysis for PS-*b*-PMMA Patterns

The difference in refractive indices (n) of the PS and PMMA materials is ~ 0.1 and the extinction coefficient values for both the polymers are close to zero from 250 to 1000 nm. There is a nearly indiscernible difference for Ψ and Δ and the MM elements between the different chemical guide pitch samples for perfectly oriented DSA PS-*b*-PMMA patterns. Also, the off-diagonal Mueller elements are close to zero for all azimuth angles. However, Ψ and Δ and the MM elements for the completely disoriented PS-*b*-PMMA patterns can be distinguished from perfectly oriented patterns, and the Mueller elements of disoriented lines are red-shifted from the Mueller elements of the perfectly oriented PS-*b*-PMMA lines as seen in Fig. 5.

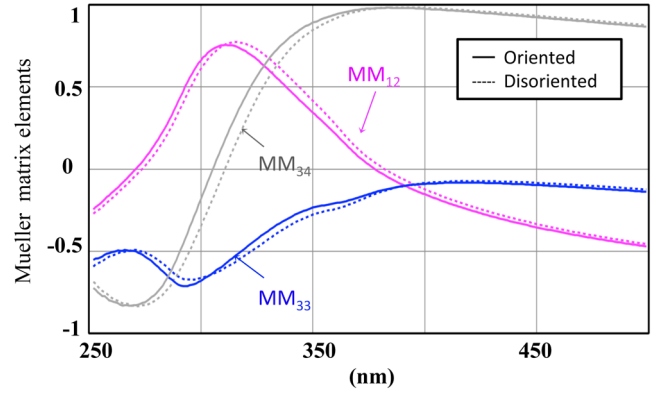


Fig. 5 Experimental Mueller matrix spectroscopic ellipsometry (MMSE) data (MM_{12} , MM_{33} , MM_{34}) collected at 0 deg azimuth from perfectly oriented and disoriented fingerprint-like polystyrene-*b*-polymethylmethacrylate patterns.

MMSE data collected from a sample have complex dependence on the topography of the structure, orientation of the structure with reference to the plane of incidence, depolarization emanated due to any nonidealities present in the structure, and optical properties associated with the grating and any layers underneath the structure.¹⁵ The optical response of the scatterometry model is fit to the experimentally measured optical spectra. The MSE is used as the criteria to estimate the degree of mismatch between experimental

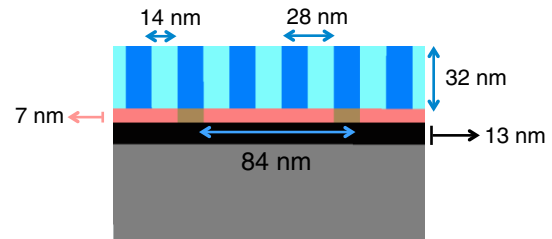


Fig. 6 Final profile of the scatterometry model for $3xL_0$ unetched sample.

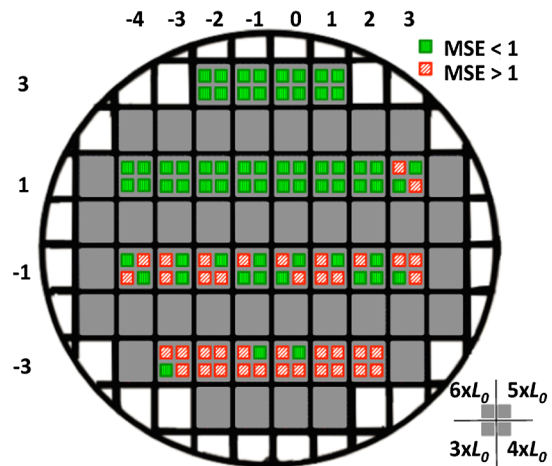


Fig. 7 Scatterometry-based wafer map for unetched samples with respect to mean squared error (MSE) obtained for data collected at 0 deg azimuthal angle.

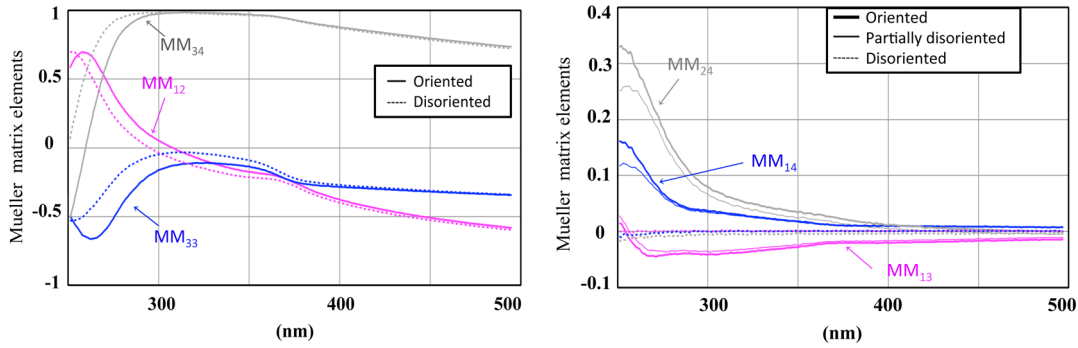


Fig. 8 (a) Experimental MMSE data (MM_{12} , MM_{33} , MM_{34}) collected at 0 deg azimuth from strongly oriented and disoriented fingerprint-like polystyrene (PS) line-space patterns. (b) Experimental MMSE data (off-diagonal elements) collected at 45 deg azimuth from strongly oriented, partially disoriented, and fingerprint-like PS line-space patterns.

and model-generated data. Scatterometry is able to differentiate between perfectly oriented and completely disoriented PS-*b*-PMMA patterns, but sensitivity to partially ordered PS-*b*-PMMA patterns is not observed for the unetched samples. MSE values for both perfectly oriented and partially disordered PS-*b*-PMMA patterns is <1 , and for fingerprint-like patterns, it is >1 . The scatterometry structural model

and the scatterometry-based wafer map for unetched DSA PS-*b*-PMMA with respect to the MSE obtained from scatterometry analysis are seen in Figs. 6 and 7, respectively.

Table 1 Mueller-based scatterometry mean squared error (MSE) values measured using NanoDiffract® software.

MSE values measured for various macros across the wafer					
Field	(0, 3)	(0, 3)	(1, -3)	(1, -3)	
angle of incidence (AOI) = 65 deg	Azimuth direction (deg)	MSE	Azimuth direction (deg)	MSE	
Macro: $3 \times L_o$	0	0.57	0	1.69	
	45	0.59	45	1.73	
	90	0.62	90	1.80	
AOI = 65 deg	Azimuth direction (deg)	Avg. MSE	Azimuth direction (deg)	Avg. MSE	
	Macro: $4 \times L_o$	0	0.61	0	1.73
		45	0.64	45	1.78
		90	0.67	90	1.82
Macro: $5 \times L_o$	0	0.61	0	1.62	
	45	0.66	45	1.79	
	90	0.70	90	1.96	
Macro: $6 \times L_o$	0	0.62	0	1.73	
	45	0.67	45	1.83	
	90	0.69	90	1.98	

2.2 Analysis for PS Line-Space Patterns

The etched sample (PMMA removed) provides better optical contrast than the unetched samples. Differences in the MM elements are seen in Fig. 8(a) for perfectly oriented and disoriented fingerprint-like PS line-space structures. A clear blue-shift is observed in MM elements with increasing disorder in the etched samples in contrast to the red-shift observed for the unetched samples. Nonzero off-diagonal Mueller elements are obtained for etched samples measured at a 45 deg azimuth, within the wavelength range between 245 and 450 nm for perfectly oriented PS line-space patterns as seen in Fig. 8(b). As pattern order decreases, the off-diagonal MM elements tend toward zero with a minimum observed for completely disordered or fingerprint-like PS line-space patterns. This trend in the off-diagonal elements is directly related to changes in the depolarization coefficient and anisotropy coefficient values, which can be directly used to measure the amount of disorder in the PS line-space patterns. The structure and CD of the underlying chemical guide pitch is essential for the directed self-assembly process.¹ In contrast to SE and CD-SEM, MMSE data are found to be sensitive to underlying chemical guide pitch for the etched samples.¹⁵

MMSE based scatterometry is more effective in characterizing the etched samples. Changes in MSE values as seen in Tables 1 and 2 are used as the criteria for estimating the degree of disorientation of PS-*b*-PMMA patterns and PS line-space patterns across the FEM wafer. For each azimuthal angle, the lowest MSE value is measured for macros containing parallel lines and increases for macros with little structural order. The differences in MSE values are large enough to routinely distinguish among ordered, partially disordered, and fingerprint-like patterns.¹⁶ The wafer map for etched samples with respect to the MSE obtained from scatterometry analysis and the structural model are seen in Figs. 9 and 10, respectively. The scatterometry results for the etched samples are found to correlate with the CD-SEM results as seen in Fig. 11.

Table 2 Mueller-based scatterometry MSE values measured using NanoDiffract® software.

MSE values measured for various macros across the wafer									
Field	(0,3)	(0,3)	(0,3)	(-2, 1)	(-2, 1)	(-2, 1)	(-2, -1)	(-2, -1)	(-2, -1)
AOI = 65 deg	Azimuth direction (deg)	Avg. MSE	Std. deviation	Azimuth direction (deg)	Avg. MSE	Std. deviation	Azimuth direction (deg)	Avg. MSE	Std. deviation
Macro: $3xL_0$	0	0.46	0.01	0	1.72	0.47	0	4.01	0.42
	45	0.99	0.01	45	2.79	0.06	45	6.13	0.04
	90	1.06	0.02	90	4.96	0.34	90	8.85	0.25
Field	(0, 3)	(0, 3)	(0, 3)	(-3, 1)	(-3, 1)	(-3, 1)	(2, -1)	(2, -1)	(2, -1)
AOI = 65 deg	Azimuth direction (deg)	Avg. MSE	Std. deviation	Azimuth direction (deg)	Avg. MSE	Std. deviation	Azimuth direction (deg)	Avg. MSE	Std. deviation
Macro: $4xL_0$	0	0.31	0.007	0	1.11	0.07	0	4.43	0.28
	45	0.49	0.01	45	2.46	0.25	45	6.78	0.29
	90	0.66	0.01	90	4.53	0.37	90	8.40	0.62
Field	(0, 3)	(0, 3)	(0, 3)	(-4, 1)	(-4, 1)	(-4, 1)	(0, -3)	(0, -3)	(0, -3)
AOI = 65 deg	Azimuth direction (deg)	Avg. MSE	Std. deviation	Azimuth direction (deg)	Avg. MSE	Std. deviation	Azimuth direction (deg)	Avg. MSE	Std. deviation
Macro: $5xL_0$	0	0.36	0.02	0	1.35	0.06	0	3.14	0.18
	45	0.60	0.008	45	3.27	0.19	45	6.32	0.26
	90	0.85	0.01	90	5.02	0.17	90	10.09	0.60
Field	(0, 3)	(0, 3)	(0, 3)	(0, 1)	(0, 1)	(0, 1)	(1, 1)	(1, 1)	(1, 1)
AOI = 65 deg	Azimuth direction (deg)	Avg. MSE	Std. deviation	Azimuth direction (deg)	Avg. MSE	Std. deviation	Azimuth direction (deg)	Avg. MSE	Std. deviation
Macro: $6xL_0$	0	0.44	0.003	0	1.92	0.11	0	4.64	0.54
	45	0.81	0.01	45	4.34	0.19	45	7.28	0.28
	90	0.93	0.02	90	5.41	0.43	90	9.87	0.46

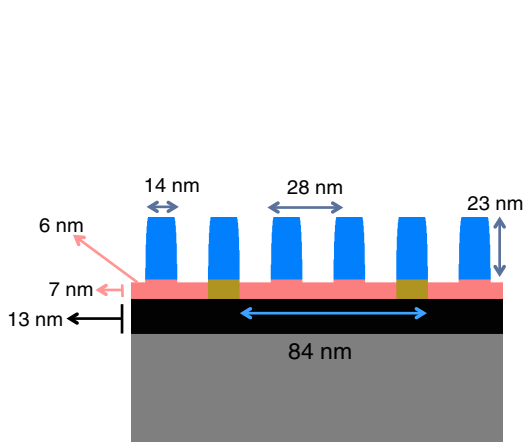


Fig. 9 Final profile of the multiparameter model for $3xL_0$ etched sample.

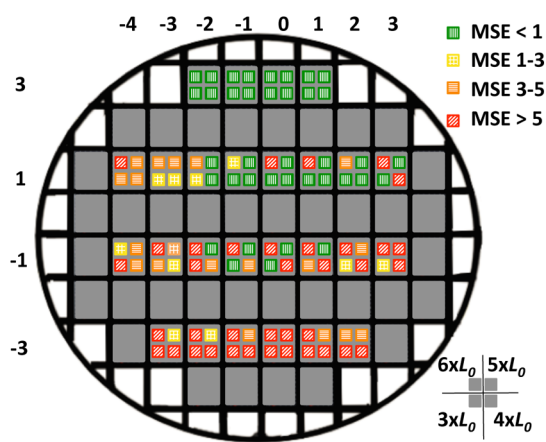


Fig. 10 Scatterometry-based wafer map for etched samples with respect to MSE obtained for data collected at 45 deg azimuthal angle.

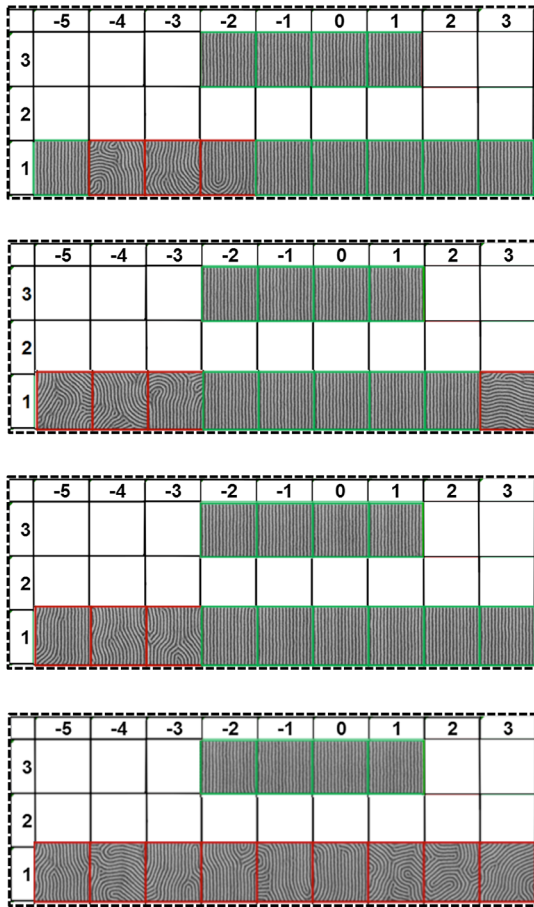


Fig. 11 Critical dimension scanning electron microscopy (CD-SEM) images for (a) $3xL_0$, (b) $4xL_0$, (c) $5xL_0$, and (d) $6xL_0$ macros.

2.2.1 Anisotropy Measurements

Anisotropy coefficients (α , β , and γ) are calculated from non-depolarizing experimental MMSE data using Eqs. (8) and (9). Calculated anisotropy coefficient values, $\alpha \approx 0$, $\beta \approx 0$, $\gamma \approx 1$, show that scattered light is circularly anisotropic for wavelengths >400 nm, at an azimuthal angle of 45 deg, and across the entire wavelength range for azimuthal angles of 0 and 90 deg. For experimental MMSE data

collected at a 45 deg azimuthal angle, due to nonzero off-diagonal Mueller matrix elements, it is observed that $\alpha \neq 0$, $\beta \neq 0$, $\gamma \neq 0$ in the wavelength range of 250 to 500 nm for perfectly oriented PS line-space patterns, and an increase in disorientation of self-assembled PS lines are correlated with a decrease in the value of α and β (to 0), while the value of γ increased to 1.¹⁶ This trend of change in anisotropy coefficients can be correlated to a change in intensity of the off-diagonal Mueller elements with a change in the degree of alignment of PS line-space patterns as shown in Fig. 8(b). A full wafer map corresponding to the changes in the circular anisotropy coefficient (γ) values measured at a 45 deg azimuth and exposed at 260 nm is seen in Fig. 12, which is very similar to the MSE wafer map shown in Fig. 9.

2.2.2 Depolarization measurements

The depolarization is the loss of coherence of the phase or the amplitude of the electric field. It is the decrease of the degree of polarization of totally polarized light after it has interacted with the medium.⁷ The depolarization coefficient is calculated directly from the experimental MMSE data using Eq. (7). It was previously reported that for all azimuthal directions, the depolarizing coefficient value increases as structural order decreases.¹⁶ The increase in depolarization coefficient is due to certain nonidealities present in PS patterns, i.e., bridging defects, wiggles, or dislocations. The wafer map showing this increase in the depolarization coefficient value at 260 nm wavelength of light is seen in Fig. 13. Comparing Figs. 10, 12, and 13, it is seen that the depolarization coefficient is more sensitive to structural changes in PS line-space patterns than either the MSE or anisotropy maps as even the macros with parallel PS line-space patterns with slight imperfections are detected, which is confirmed by CD-SEM imaging.

2.3 Analysis for Si Fin Samples

The etch process across-wafer uniformity used for transferring the patterns for this sample is immature and, hence, a variation in the quality of Si fins is observed [i.e., the Si fins at the center of the wafer have minimum low-frequency line edge roughness (LER), while the fins at the edges have higher LER]. An unetched layer of SiN is present on top of

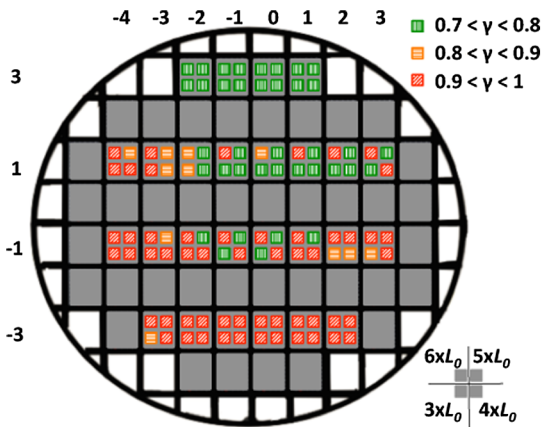


Fig. 12 Wafer map for etched samples with respect to circular anisotropy coefficient (γ) calculated from depolarization free experimental data collected at 45 deg azimuth.

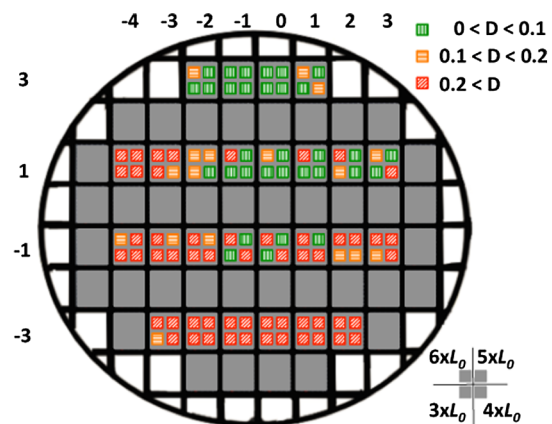


Fig. 13 Wafer map for etched samples with respect to depolarization coefficient values at 260 nm.

the Si fins and the depth of the trenches between the fins varies across the sample. This is confirmed by the cross-sectional TEM imaging of the sample.

Top down SEM images and distinct differences in the experimental MM elements acquired at a 90-deg azimuthal angle for oriented Si fins, oriented Si fins with defects and increased roughness, and fingerprint-like Si fins are seen in Figs. 14 and 15, respectively. As observed for PS line-space patterns, the off-diagonal Mueller elements are nonzero for data collected at a 45 deg azimuthal angle, and as the roughness in the Si fins increases, the MM elements tend toward zero with a minimum observed for completely disordered or fingerprint-like Si fin patterns.¹⁷

Three distinct structural models, linear Si fins, Si fins with sidewalls having optical properties modeled using an effective medium approximation (EMA), and multiparameter Si fins with periodic wiggles, are used for the scatterometry analysis and evaluation of the pattern imperfections in the Si fin samples.¹⁷ The experimental MMSE data changes drastically with the azimuthal angle. The Mueller spectrum taken at each individual azimuth is already sufficient to reconstruct the profile by fitting data with a simple model. Model verification is performed by examining spectra obtained at different azimuthal angles. The angular dependence of the MSE value is observed for both the linear fin structural model as well as EMA based model. The azimuthal angular dependence of the MSE data obtained using the linear fin structural model is used to diagnose the presence of pattern imperfections in the line array. Large differences between fit qualities at different azimuths indicate that the model does not approximate the real structure. The MSE value obtained for the multiparameter Si fin model with periodic wiggles has the advantage of being insensitive to the azimuthal angle used during measurement as seen in Fig. 16. The final profile of the multiparameter Si fin model with periodic wiggles used for the scatterometry analysis is seen in Fig. 17.

The periodicity of the wiggles is fixed at multiples of L_o to simplify the structure of the model, out of which the lowest MSE is measured at 56 nm. The MSE values reported for the well-aligned DSA-BCP PS line arrays are typically <1. Although the MSE values for the multiparameter Si fin structural model are insensitive to the azimuthal angle, the values are ~2.5. This is attributed to the use of wiggles with a fixed period of 56 nm to approximately model the nonidealities in the Si fins.

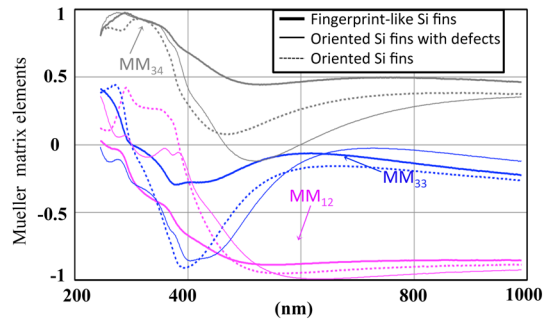


Fig. 15 Experimental MMSE data (MM_{12} , MM_{33} , MM_{34}) collected at 90 deg azimuth from oriented Si fins, oriented Si fins with defects, and fingerprint-like Si fin patterns.

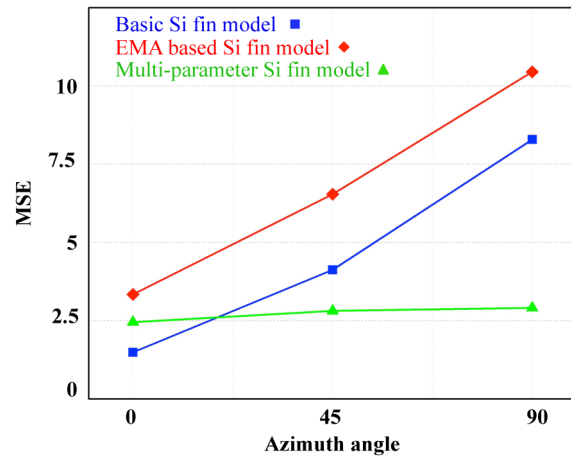


Fig. 16 MSE obtained using each model for data collected at 0, 45, and 90 deg azimuth angles.

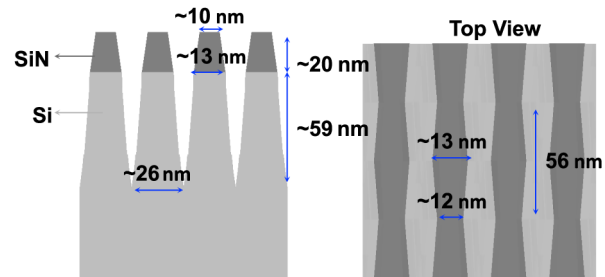


Fig. 17 Final profile of the multiparameter Si fin structural model.

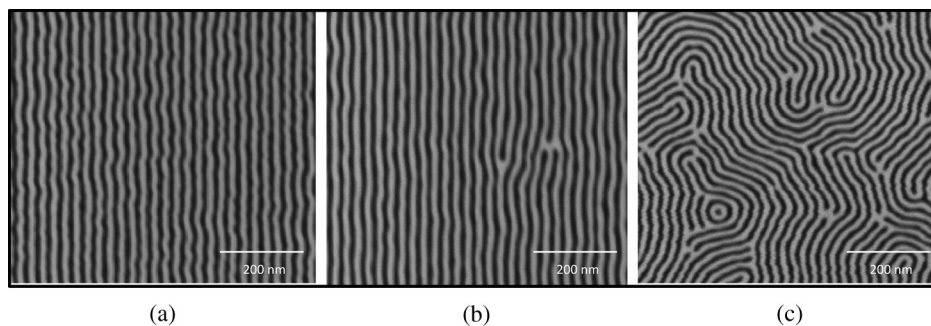


Fig. 14 Top down SEM images of (a) oriented Si fin patterns, (b) oriented Si fin patterns with defects and increased roughness, and (c) fingerprint-like Si fin patterns.

3 Discussion

MMSE-based scatterometry has the capability of measuring important feature dimensions of unetched polymer samples and is able to differentiate between perfectly oriented and completely disoriented PS-*b*-PMMA patterns, but sensitivity to partially ordered PS-*b*-PMMA patterns is not observed for the unetched samples. These results have been demonstrated here with 28 nm pitch PS-*b*-PMMA. Scatterometry is more effective in characterizing the line-space patterns where part of the polymer has been selectively removed and is also effective for Si fins. This is determined by comparing scatterometry wafer maps for unetched samples, etched samples, and CD-SEM wafer map. Sensitivity to structural parameters, such as line-width, line-shape, and even the underlying guide pitch, is observed for etched samples. Samples with different guide pattern pitches are all distinguished for fully aligned line patterns and, additionally, the amount of disorder in the patterns is measured. Anisotropy coefficients calculated from experimental MMSE data suggest that the PS line-space patterns are circularly anisotropic ($\alpha \approx 0$, $\beta \approx 0$, $\gamma \approx 1$). Incorporating anisotropic optical properties in scatterometry models is challenging, but possible, and will be the subject of future investigation. The spectral comparison based on optical anisotropy and depolarization was found to be sensitive to DSA pattern defectivity and is easy-to-use. Changes in the circular anisotropy coefficient (γ) and depolarization coefficient (D) with increasing disorientation are used to characterize the degree of disorder in the PS line-space patterns. Slight imperfections in the PS line-space patterns are detected by changes in depolarization values. Profile details of the Si fins can be measured, and sensitivity to the nonidealities present in the fin samples, such as low-frequency roughness and uneven depth, is observed.

4 Summary

Process control for BCP DSA based patterning requires advances in CD metrology and defect detection. The potential for using MMSE-based scatterometry, a nondestructive measurement technique to provide metrology for developing, monitoring, and controlling the DSA lithographic patterning process, is demonstrated. MMSE-based scatterometry has the capability to extract profile details of DSA structures (PS-*b*-PMMA patterns, PS line-space patterns, and Si fins) quickly and accurately at multiple steps in the patterning process. Additionally, the changes in MSE, anisotropy, and depolarization values are used as a quick

and efficient method to judge the degree of alignment of the DSA patterns across the wafer without substantial CD-SEM resources.

Acknowledgments

We acknowledge funding from SRC GRC under task 2337.002. We are thankful to GLOBALFOUNDRIES for providing us with the samples and Nanometrics Inc. for the help with scatterometry modeling and analysis. We would also like to acknowledge the technical support by J.A.Woollam Inc.

References

1. G. Schmid et al., "Fabrication of 28 nm pitch Si fins with DSA lithography," *Proc. SPIE* **8680**, 86801F (2013).
2. T. Novikova et al., "Application of Mueller polarimetry in conical diffraction for critical dimension measurements in microelectronics," *Appl. Opt.* **45**(16), 3688–3697 (2006).
3. M. Lazzari, G. Liu, and S. Lecommandoux, *Block Copolymers in Nanoscience*, WILEY-VCH Verlag GmbH&Co., Weinheim (2006).
4. C. Liu et al., "Chemical patterns for directed self-assembly of lamellae-forming block copolymers with density multiplication of features," *Macromolecules* **46**(4), 1415–1424 (2013).
5. J. Y. Cheng et al., "Simple and versatile methods to integrate directed self-assembly with optical lithography using a polarity-switched photoresist," *ACS Nano* **4**(8), 4815–4823 (2010).
6. D. P. Sanders et al., "Integration of directed self-assembly with 193 nm lithography," *J. Photopolym. Sci. Technol.* **23**(1), 11–18 (2010).
7. H. Fujiwara, *Spectroscopic Ellipsometry: Principles & Applications*, John Wiley & Sons Ltd., Sussex (2007).
8. G. Muthinti et al., "Mueller based scatterometry measurement of nanoscale structures with anisotropic in-plane optical properties," *Proc. SPIE* **8681**, 86810M (2013).
9. A. Laskarakis et al., "Mueller matrix spectroscopic ellipsometry: formulation and application," *Thin Solid Films* **455**, 43–49 (2004).
10. M. G. Moharam and T. K. Gaylord, "Rigorous coupled-wave analysis of planar-grating diffraction," *J. Opt. Soc. Am.* **71**(7), 811–818 (1981).
11. J. J. Gil and E. Bernabeu, "A depolarization criterion in Mueller matrices," *Opt. Acta: Int. J. Opt.* **32**(3), 259–261 (1985).
12. J. J. Gil and E. Bernabeu, "Depolarization and polarization indices of an optical system," *Opt. Acta: Int. J. Opt.* **33**(2), 185–189 (1986).
13. O. Arteaga, E. Garcia-Caurel, and R. Ossikovski, "Anisotropy coefficients of a Mueller matrix," *J. Opt. Soc. Am.* **28**(4), 548–553 (2011).
14. R. Ossikovski et al., "Depolarizing Mueller matrices: how to decompose them," *Physica Status Solidi (A)* **205**(4), 720–727 (2008).
15. T. Novikova et al., "Metrological applications of Mueller polarimetry in conical diffraction for overlay characterization in microelectronics," *Eur. Phys. J. Appl. Phys.* **31**, 63–69 (2005).
16. D. Dixit et al., "Metrology for directed self-assembly block lithography using optical scatterometry," *Proc. SPIE* **9050**, 90500N (2014).
17. D. Dixit et al., "Mueller matrix optical scatterometry of Si fins patterned using directed self-assembly block copolymer line arrays," in *25th Annual SEMI Advanced Semiconductor Manufacturing Conf.*, pp. 180–185 (2014).

Biographies of the authors are not available.